Perioperative evaluation of regional aortic wall shear stress patterns in patients undergoing aortic valve and/or proximal thoracic aortic replacement

Emilie Bollache, PhD,[a] Paul W. M. Fedak, MD, PhD,[b,c] Pim van Ooij, PhD,[d] Ozair Rahman, MD,[a] S. Chris Malaisrie, MD,[c] Patrick M. McCarthy, MD,[c] James C. Carr, MD,[a] Alex Powell, MS,[a] Jeremy D. Collins, MD,[a] Michael Markl, PhD,[a,e] and Alex J. Barker, PhD[a]

ABSTRACT

Objectives: To assess in patients with aortopathy perioperative changes in thoracic aortic wall shear stress (WSS), which is known to affect arterial remodeling, and the effects of specific surgical interventions.

Methods: Presurgical and postsurgical aortic 4D flow MRI were performed in 33 patients with aortopathy (54 ± 14 years; 5 women; sinus of Valsalva (d_SOV)/midascending aortic (d_MAA) diameters = 44 ± 5/45 ± 6 mm) scheduled for aortic valve (AVR) and/or root (ARR) replacement. Control patients with aortopathy who did not have surgery were matched for age, sex, body size, and d_MAA (n = 20: 52 ± 14 years; 3 women; d_SOV/d_MAA = 42 ± 4/42 ± 4 mm). Regional aortic 3D systolic peak WSS was calculated. An atlas of WSS normal values was used to quantify the percentage of at-risk tissue area with abnormally high WSS, excluding the area to be resected/graft.

Results: Peak WSS and at-risk area showed low interobserver variability (≤0.09 [−0.3; 0.5] Pa and 1.1% [−7%; 9%], respectively). In control patients, WSS was stable over time (follow-up–baseline differences ≤0.02 Pa and 0.0%, respectively). Proximal aortic WSS decreased after AVR (n = 5; peak WSS difference ≤−0.41 Pa and at-risk area ≤−10%, $P < .05$ vs controls). WSS was increased after ARR in regions distal to the graft (peak WSS difference ≥0.16 Pa and at-risk area ≥4%, $P < .05$ vs AVR). Follow-up duration had no significant effects on these WSS changes, except when comparing ascending aortic peak WSS between ARR and AVR ($P = .006$).

Conclusions: Serial perioperative 4D flow MRI investigations showed distinct patterns of postsurgical changes in aortic WSS, which included both reductions and translocations. Larger longitudinal studies are warranted to validate these findings with clinical outcomes and prediction of risk of future aortic events. (J Thorac Cardiovasc Surg 2018;155:2277-86)

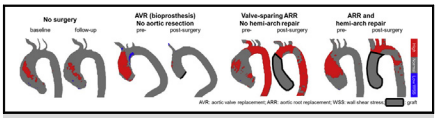

Changes in at-risk tissue (*red*) for control (no surgery) and aortic surgery patients.

Central Message

Differing proximal aorta interventions induced distinct changes in wall shear stress (WSS). Further research is needed to validate 4D flow MRI WSS to predict outcome and inform surgical practice.

Perspective

Changes between presurgical and postsurgical aortic wall shear stress in the face of different interventions (valve and/or root replacement with or without hemiarch repair) are reported herein for the first time. Given the potential role of hemodynamics on the progression of aortopathy, this noninvasive imaging biomarker may identify patients at high risk for future events and optimize operative strategies.

See Editorial Commentary page 2287.

See Editorial page 2252.

Patients with thoracic aortic disease are often asymptomatic before acute critical events such as dissection or rupture occur. Early detection and management are necessary to minimize risk. When necessary, prophylactic surgical repair or replacement of the aorta and/or aortic valve is recommended. Risk for these events is assessed from diameter

Scanning this QR code will take you to a supplemental video and figure for this article.

From the [a]Department of Radiology, Feinberg School of Medicine, [c]Division of Surgery-Cardiac Surgery, and [e]Department of Biomedical Engineering, McCormick School of Engineering, Northwestern University, Chicago, Ill; [b]Department of Cardiac Sciences, Cumming School of Medicine, University of Calgary, Calgary, Alberta, Canada; and [d]Department of Radiology, Academic Medical Center, Amsterdam, The Netherlands.

This work was supported by the National Institutes of Health grants R01HL115828 and K25HL119608 as well as the American Heart Association Midwest Affiliate grant 16POST27250158.

Received for publication June 27, 2017; revisions received Oct 11, 2017; accepted for publication Nov 6, 2017; available ahead of print Dec 14, 2017.

Address for reprints: Alex J. Barker, PhD, Department of Radiology, Feinberg School of Medicine, Northwestern University, 737 N Michigan Ave, Suite 1600, Chicago, IL 60611 (E-mail: Alex.barker@northwestern.edu).

0022-5223/$36.00

https://doi.org/10.1016/j.jtcvs.2017.11.007

Abbreviations and Acronyms

2D	= two-dimensional
3D	= three-dimensional
4D flow MRI	= three-dimensional time-resolved phase-contrast magnetic resonance imaging with three-directional velocity encoding
AA	= ascending aorta
ARR	= aortic root replacement
AVR	= aortic valve replacement
BAV	= bicuspid aortic valve
CE-MRA	= contrast-enhanced magnetic resonance angiography
DA	= descending aorta
ECG	= electrocardiogram
HA	= hemiarch repair
LV	= left ventricle
LVEF	= left ventricular ejection fraction
LVSV	= left ventricular stroke volume
MRI	= magnetic resonance imaging
PC	= phase-contrast
SOV	= sinus of Valsalva
VS-ARR	= valve-sparing ARR
WSS	= wall shear stress

measurements provided by computed tomography, magnetic resonance imaging (MRI) or echocardiography.[1] However, efforts to use advanced noninvasive imaging to risk-stratify these patients have been proposed.[2] For example, the measurement of three-dimensional (3D) cine (time-resolved) blood flow with three-directional velocity encoding (known as 4D flow MRI) has enabled the use of noninvasive MRI to investigate complex hemodynamics and 3D blood flow patterns.

Previous quantitative in vivo evaluations of postoperative aortic hemodynamics in the literature have mostly focused on transvalvular gradients,[3-8] valvular regurgitation,[3,4,9-11] or peak velocity.[9,12,13] In addition, wall shear stress (WSS), defined as the tangential viscous force exerted by blood flow on the arterial wall, is an important potential biomarker, because it plays a major role in the regulation of cellular function and remodeling via endothelial mechanotransduction.[14] For example, aortic WSS has been studied using 4D flow MRI after valve-sparing aortic root replacement (VS-ARR) in patients with Marfan syndrome[15] or bicuspid aortic valve (BAV).[16] It has also been used to compare different types of valve prosthesis after aortic valve replacement (AVR)[17] or in the evaluation of the impact of surgical and transcatheter AVR procedures.[18] A 4D flow MRI study in patients with BAV has shown that aortic regions with abnormally increased WSS had significant alterations of elastin fibers and extracellular matrix proteins implicated in aortic wall degeneration.[19]

Studies have also investigated perioperative findings of aortic hemodynamics, but they primarily focused on valvular regurgitation,[10,20] pressure gradient,[7,10] or peak velocity,[20] mainly in the setting of AVR. Two studies have reported on WSS changes between preintervention and after surgical[21] or transcatheter[22] AVR, with a focus on investigating carotid and brachial WSS, respectively. However, no comprehensive study has investigated preoperative and postoperative aortic hemodynamic WSS data beyond that of AVR alone. Thus, the purpose of this study is to compare presurgical and postsurgical aortic WSS patterns in patients with aortopathy who underwent replacement of the aortic valve and/or the aorta, using 4D flow MRI. Follow-up 4D flow MRI data of patients with aortopathy who did not have surgery were also investigated as controls. Our hypothesis is that surgery affects WSS, with different changes according to the performed intervention.

METHODS

Study Population

All patients were identified, via institutional review board–approved retrospective chart review with a waiver of consent, from a 4D flow MRI database with 1673 patients (ie phase-contrast MRI with velocity encoding in all 3 spatial directions that is resolved relative to all 3 dimensions of space [3D] and to the dimension of time [cine] along the cardiac cycle). We selected all patients with aortic and/or valve disease (n = 1128). Among them, we included the 244 who had undergone aortic valve and/or aorta replacement as well as postoperative clinically ordered standard-of-care cardiothoracic MRI, including 4D flow. We further identified patients who also had undergone a 4D flow examination before surgery (n = 55). We excluded those with a history of aortic dissection or previous aortic interventions (n = 21), as well as a single patient who underwent a modified Ross pulmonary autograft procedure, resulting in 33 patients and 66 MRI data sets. A consort flow diagram is provided in the Figure E1. In addition, 20 control patients with aortopathy matched for age, gender, height, and weight, who underwent baseline and follow-up routine surveillance MRI (n = 40 data sets) but no surgery in between, were included.

Surgical Procedures

All operations were performed between 2012 and 2016.

VS-ARR was performed using a modified reimplantation technique, with a 34-mm Dacron graft. Coronary reconstruction was achieved with reimplantation of left and right coronary arteries as buttons, with a concomitant valve repair for all cases. A second smaller 24-mm to 28-mm graft was used to replace the tubular segment of the ascending aorta (AA). A large straight graft was used for the sinus portion.

ARR with concomitant AVR was performed using a modified Bentall procedure. The valve was sewn into a 7-mm larger Gelweave Dacron graft (VASCUTEK, Inchinnan, United Kingdom). The annular sutures were passed through the valve conduit. The left main and right coronary ostia were anastomosed as buttons to the side of the conduit.

Further hemiarch repair (HA), involving resection of the aorta up to its distal end from the base of the innominate artery to the lesser curve,[23] was performed when the diameter of the proximal aortic arch was >4 cm.

In ARR combined with AVR as well as AVR alone procedures, different valve prostheses were used: bioprosthesis (23-mm to 29-mm Carpentier-Edwards pericardial PERIMOUNT or 23-mm to 27-mm Carpentier-Edwards pericardial Magna Ease or 27-mm to 29-mm Edwards INTUITY bovine pericardial valve [Edwards Lifesciences, Irvine, Calif]) or a mechanical valve (23-mm to 27-mm On-X valve; CryoLife Inc, Kennesaw, Ga).

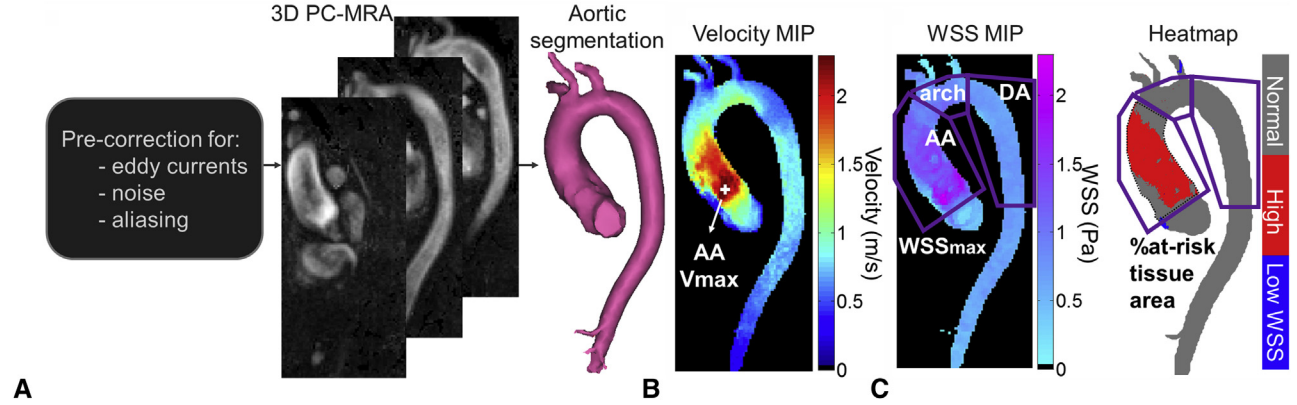

FIGURE 1. Analysis of aortic 4D flow MRI (three-dimensional time-resolved phase-contract magnetic resonance imaging with three-directional velocity encoding) data. A, Preprocessing, calculation of the three-dimensional phase-contrast angiogram (*3D PC-MRA*) and segmentation of the aortic volume. B, Estimation of systolic peak velocity (location indicated by the *white marker,* V_{max}) in the vena contracta, from velocity maximal intensity projections (*MIP*). C, Evaluation of wall shear stress (*WSS*) patterns along the ascending aorta (*AA*), arch, and descending aorta (*DA*) wall (*purple regions of interest*): (1) systolic peak magnitude (WSSmax) provided by the WSS MIP; (2) at-risk tissue percentage area, defined as regions with a WSS above normal values (mean + 1.96 × standard deviation of WSS atlas values averaged over a group of 56 healthy volunteers) provided by the heatmap (*red*). The *dotted line* on the heatmap indicates the area to be resected.

For each intervention, perfusion time, cross-clamp time, and postoperative length of stay were recorded.

MRI Acquisitions

All baseline and follow-up MRI examinations were performed between 2011 and 2016.

Examination acquisition included electrocardiogram (ECG)–gated two-dimensional (2D) cine balanced steady-state free precession images for the evaluation of cardiac volumes and function (left ventricular [LV] stroke volume [LVSV] and ejection fraction [LVEF]), as well as contrast-enhanced magnetic resonance angiography (CE-MRA) of the thoracic aorta for aortic dimension characterization (sinuses of Valsalva [SOVs] and mid-AA diameters). Furthermore, 2D cine through-plane phase-contrast MRI was performed at the aortic valve, for aortic valve disease evaluation (BAV morphology Sievers classification and severity of stenosis and regurgitation). Aortic 4D flow MRI was performed to subsequently derive peak velocity and WSS. Details regarding MRI acquisition parameters and data analysis are provided in the Appendix E1.

Quantification of Baseline and Follow-up Aortic WSS Patterns From 4D Flow MRI Data

The analysis of each baseline and follow-up 4D flow MRI data set, including preprocessing, calculation of a 3D angiogram, and aortic segmentation, is shown in Figure 1, *A*, and detailed in the Appendix E1.

Maximum intensity projections of the systolic absolute velocities inside the 3D segmentation were calculated and used to obtain the peak velocity in the vena contracta (Figure 1, *B*), using a previously described approach.[24]

WSS, defined as the product between blood dynamic viscosity and the velocity spatial gradient at the wall, was calculated throughout the entire 3D aortic surface using an in-house MATLAB algorithm.[25] In particular, systolic WSS was averaged over 5 cardiac phases centered on the peak systolic phase, as defined by the time phase with the highest velocity averaged within the segmented aortic volume. Furthermore, aortic heatmaps were created, using a healthy control atlas previously established in 56 controls representing the 95% confidence interval of the normal WSS range.[26] For each patient and each baseline and follow-up 4D flow data set, WSS 3D distribution was registered to this atlas, to identify regions with an abnormally increased WSS (ie above the 95% confidence interval). Regional WSS patterns were then characterized in the AA, the aortic arch, and the proximal descending aorta (DA). The AA was defined by the region between the aortic valve and the first supra-aortic vessel, the aortic arch included the region between the first and last supra-aortic vessels, and the proximal DA comprised the region from the last supra-aortic vessel takeoff to the corresponding level of the aortic valve. For each AA, arch, and DA region (Figure 1, *C*): (1) peak WSS magnitude (averaged over the 2% highest values) and (2) at-risk tissue area exposed to abnormally high WSS, calculated from the heatmap red regions and further expressed in percentage of the total area, were extracted. In patients undergoing surgery, the area to be resected and the graft, before and after surgery, respectively, were excluded from WSS analyses as visually evaluated using CE-MRA or computed tomography angiography images when available. Thus, WSS indices were studied in the aortic arch and DA for all patients, and, in patients who underwent ARR, only in the AA region that was not replaced. In addition, total at-risk tissue absolute area in the whole aorta of no-surgery patients was also reported.

Interobserver Reproducibility

To assess their sensitivity to segmentation and their reproducibility, peak WSS magnitude and percentage at-risk tissue area were calculated from both baseline and follow-up data sets using aortic volume segmented by 2 blinded and independent operators in 10 randomized controls (including 5 patients with a tricuspid aortic valve and 5 patients with a BAV) and 10 randomized surgery patients (including 2 patients who underwent AVR alone, 5 patients who underwent ARR with no HA and 3 patients who underwent ARR and HA).

Statistical Analysis

Normal distributions were tested using a Lilliefors test. Data are reported as mean ± standard deviation when their distribution was normal or otherwise as median (interquartile range). Follow-up duration and longitudinal changes in WSS indices were further studied in surgery subgroups according to the aortic valve type and performed intervention. Comparisons between patient groups were performed using a Wilcoxon rank-sum test, and differences between baseline and follow-up were tested using a Wilcoxon signed-rank test. We further investigated longitudinal WSS pattern changes as defined as follow-up minus baseline peak WSS

TABLE 1. Baseline characteristics, aortic valve and left ventricular function and aortic diameters, as well as follow-up durations according to patient group

	No surgery (n = 20)	Surgery (n = 33)
Women, n (%)	3 (15)	5 (15)
Age (years), mean ± SD	52 ± 14	54 ± 14
Height (cm), mean ± SD	178 ± 9.4	175 ± 10
Weight (kg), mean ± SD	89 ± 15	87 ± 15
BAV, n (%)	10 (50)	25 (76)
Type 0		
ap, n	1	3
lat, n	2	2
Type 1		
LR, n	5	12
RN, n	1	4
Type 2: LR/RN, n	1	4
AS: none/trace/mild/moderate/severe, n	19/0/1/0/0	16/7/2/6/2
AI: none/trace/mild/moderate/severe, n	5/5/8/2/0	5/7/12/6/3
SOV diameter (mm), mean ± SD	41.8 ± 4.1	44.0 ± 5.2
Mid-AA diameter (mm), mean ± SD	41.8 ± 4.0	45.2 ± 6.3*
SBP/DBP (mmHg), mean ± SD	128 ± 13/77 ± 8.9	128 ± 16/77 ± 13
LV SV (mL), mean ± SD	85 ± 22	105 ± 36
LV EF (%), mean ± SD	62 ± 7.2	60 ± 8.6
Heart rate (bpm), mean ± SD	65 ± 8.6	69 ± 14
MRI follow-up duration (days), median (interquartile range)	854 (419-1067)	48 (26-191)*
Baseline MRI to surgery, days, median (interquartile range)	—	21 (15-49)
Surgery to follow-up MRI days, median (interquartile range)	—	6 (4-20)

SD, Standard deviation; *BAV*, bicuspid aortic valve; *ap*, anterior-posterior; *lat*, lateral; *LR*, left-right coronary sinus; *RN*, right-noncoronary sinus; *AS*, aortic stenosis; *AI*, aortic insufficiency; *SOV*, sinus of Valsalva; *AA*, ascending aorta; *SBP*, systolic blood pressure; *DBP*, diastolic blood pressure; *LV*, left ventricular; *SV*, stroke volume; *EF*, ejection fraction; *MRI*, magnetic resonance imaging. *$P < .05$ between surgery and no-surgery groups.

and percentage at-risk tissue area differences. Differences in WSS change between patient groups were studied using linear mixed-effects models, taking into account baseline WSS measurement, patient category (surgery vs no surgery or intervention type), and follow-up duration. Interobserver variability was studied using Bland-Altman analyses and mean biases and limits of agreement (as defined as mean ± 1.96* standard deviation) were provided. A value $P < .05$ was considered as statistically significant. Statistical analyses were performed using MATLAB (MathWorks, Natick, Mass).

RESULTS

Patient Baseline Characteristics and Surgery Details

Patient baseline characteristics are summarized for the surgery and no-surgery groups in Table 1. SOV diameter was similar between the 2 patient groups, but, as expected, the mid-AA was significantly more dilated in patients undergoing surgery. LVSV and LVEF were similar between the 2 groups. The median MRI follow-up duration was significantly longer for no-surgery (range, 1-4 years) than surgery patients (1 week to 3.3 years). Duration between baseline MRI and surgery ranged from 1 day to 3.3 years, whereas surgery to follow-up MRI duration ranged from 2 days to 2.6 years. At follow-up, changes in LVSV and LVEF were insignificant compared with baseline in both patient groups (91 ± 29 mL/92 ± 21 mL and 59 ± 12%/58 ± 8.7% in no-surgery/surgery patients, respectively; differences were insignificant between the 2 groups).

Subgrouping of surgery patients was further performed according to the intervention type and valve prosthesis, as shown in Table 2: 5 patients had AVR with no resection of the aorta. Among the remaining 28 patients who had ARR, 22 had concomitant AVR and 12 had further HA (ARR-HA^{+}). Median valve size was 27 mm (interquartile range, 25-27 mm), maximum conduit size was 34 mm (34-34 mm), hemiarch graft size was 26 mm (25-26 mm), mean perfusion time was 143 ± 53 min, cross-clamp time was 122 ± 44 min, and median postoperative length of stay was 5 days (interquartile range, 4-6 days). Follow-up surveillance time is further provided for each subgroup, showing significantly longer durations for the AVR-alone group versus all other surgery ARR patients with or without HA ($P < .01$).

Longitudinal Evolution of WSS Patterns

Video 1 provides an example of blood flow patterns in the proximal aorta provided by 4D flow MRI at pre- and postsurgery in a patient who underwent AVR with a

TABLE 2. Summary of performed interventions and replaced aortic valve types in the surgery group. Baseline to follow-up magnetic resonance imaging duration as well as surgery to follow-up magnetic resonance imaging duration (days) are provided for each subgroup

	AVR alone (n = 5)	ARR-HA$^-$ (n = 16)	ARR-HA$^+$ (n = 12)
Bioprosthesis, n	4	12	6
MRI f-u duration (days), median (interquartile range)	408 (334-594)	43 (27-102)	32 (20-40)
Surgery to f-u MRI (days), median (interquartile range)	380 (321-559)	6 (5-18)	6 (5-17)
Mechanical valve, n	1	0	4
MRI f-u duration (days), median (interquartile range)	141	—	56 (33-72)
Surgery to f-u MRI (days), median (interquartile range)	92	—	4 (3-5)
VS-ARR, n		4	2
MRI f-u duration (days), median (interquartile range)	—	33 (20-45)	191; 1200
Surgery to f-u MRI (days), median (interquartile range)		4 (3-9)	6; 3

AVR, Aortic valve replacement; *ARR-HA*$^-$, aortic root replacement with no hemiarch repair; *ARR-HA*$^+$, aortic root replacement and hemiarch repair; *MRI*, magnetic resonance imaging; *f-u*, follow-up; *VS-ARR*, valve-sparing aortic root replacement.

bioprosthesis. Figures 2, *A,* and 3, *A*, show baseline and follow-up aortic WSS magnitude maximum intensity projection and heatmaps, respectively, in representative control and surgery patients by intervention and aortic valve type. The evolution over time of regional peak WSS and at-risk tissue percentage area is provided in Figures 2, *B,* and 3, *B*, respectively.

In the no-surgery control group, the median total absolute area of aortic at-risk tissue was 1.4 cm^2 (interquartile range, 0.4-5.4 cm^2) and 1.7 cm^2 (0.1-13 cm^2) at baseline and follow-up, respectively ($P = .57$). In surgery patients, median preintervention at-risk tissue area was 3.2 cm^2 (interquartile range, 0.0-36 cm^2) (nonsignificant vs controls). After surgery, it was 7.8 cm^2 (1.9-21 cm^2) (nonsignificant vs preintervention area and vs controls at follow-up). No significant regional differences between baseline and follow-up were observed for both aortic WSS indices in both patient groups (Table 3) or in surgery subgroups according to the intervention type. Although both AA peak WSS and at-risk tissue area were similar between no-surgery and surgery patients at baseline, they were significantly higher in the latter group after intervention. We also observed increased WSS indices in surgery patients in the aortic arch at both baseline and follow-up, compared with controls. DA peak WSS was significantly higher than controls in surgery patients at baseline and was then normalized after intervention.

Quantitative differences between follow-up and baseline confirmed unchanged WSS indices in no-surgery patients (Figures 2, *B*, and 3, *B*). It further showed a significant decrease in AA and arch peak WSS in patients who underwent AVR alone compared with changes in controls ($P \leq .008$), as well as a significant increase in patients undergoing ARR compared with changes with AVR alone ($P \leq .0008$). Follow-up duration had no significant effects on these WSS changes, except when comparing the ARR-HA$^-$ and AVR groups in the AA ($P = .006$). Similar tendencies were found for at-risk tissue area albeit restricted to the AA. No significant differences were observed between ARR-HA$^-$ and ARR-HA$^+$.

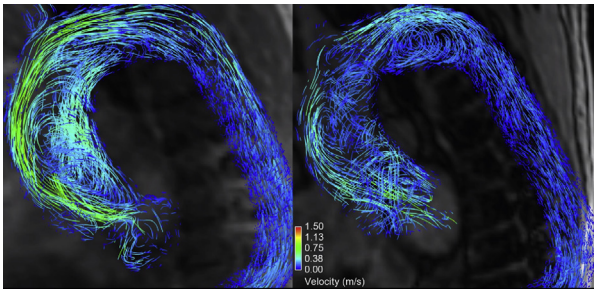

VIDEO 1. Comparison of blood flow patterns in the proximal aorta provided by 4D flow MRI (three-dimensional time-resolved phase-contrast magnetic resonance imaging with three-directional velocity encoding) before and after surgery (*left* and *right*, respectively), in a 71-year-old man with bicuspid aortic valve. The patient underwent aortic valve replacement with a 27-mm Edwards INTUITY bovine pericardial valve for moderate to severe aortic valve stenosis and mild insufficiency. In this case, blood flow was altered with reduced velocities and shear stress at the wall, suggesting blood flow pattern normalization after aortic valve replacement. Video available at: http://www.jtcvsonline.org/article/S0022-5223(17)32501-1/fulltext.

Interobserver Variability in WSS Patterns Evaluation

Interoperator biases and limits of agreement for aortic WSS patterns assessed on the 40 data sets are provided in Table 4, indicating good reproducibility.

DISCUSSION

Our main findings are (1) peak WSS and at-risk tissue area decreased after surgery in patients who had AVR alone with a bioprosthesis; (2) WSS patterns were increased distal to the graft after ARR; (3) no significant difference in WSS changes was observed within the ARR group when HA was performed or not; and (4) WSS indices showed high

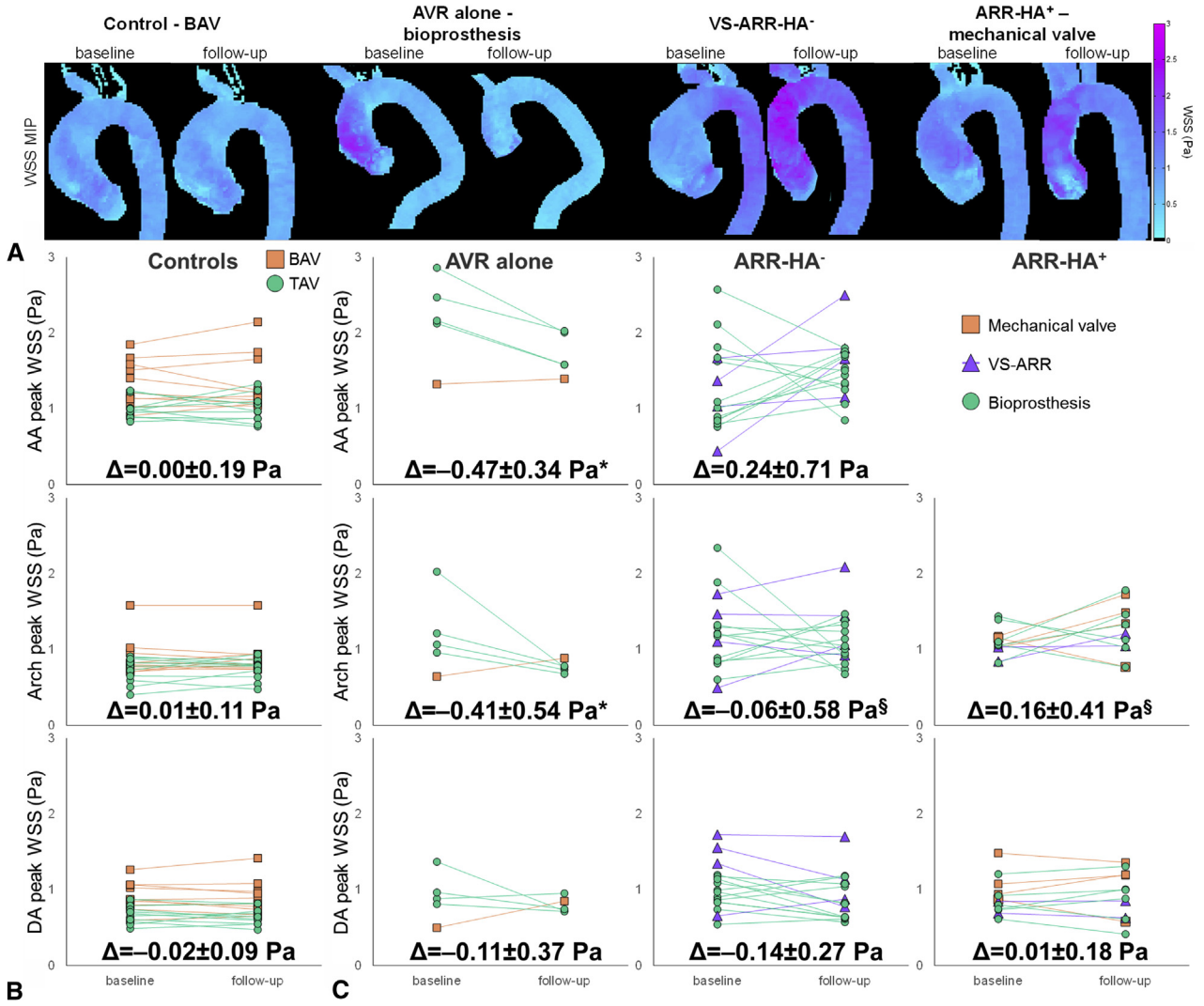

FIGURE 2. A, Baseline and follow-up aortic wall shear stress (*WSS*) magnitude maximal intensity projection (MIP) in representative control and surgery patients who underwent different intervention and aortic valve types, from left to right: bicuspid aortic valve (*BAV*) control, aortic valve replacement (*AVR*) alone with a bioprosthesis, valve-sparing aortic root replacement (*ARR*) with no hemiarch repair (HA) (*VS-ARR-HA*$^{-}$) and ARR with HA (*ARR-HA*$^{+}$) with a mechanical valve. B, Evolution of peak WSS magnitude from baseline to follow-up in the control and (C) the surgery groups according to aortic valve type (see legends). The surgery group was further divided according to the performed intervention, from left to right: AVR alone, ARR-HA^{-}, and ARR-HA+. Longitudinal changes (Δ), as defined by follow-up–baseline differences, are provided for each patient group and aortic region: ascending aorta (*AA*, *top row*), aortic arch (*middle row*) and descending aorta (*DA*, *bottom row*). Results were not reported in the AA for the ARR-HA^{+} group because the entire region was resected during surgery. *$P < .05$ against control group, §$P < .05$ against AVR group, with nonsignificant effects of follow-up duration. *TAV*, Tricuspid aortic valve.

interobserver reproducibility and remained consistent over time in patients without surgery.

Previous studies have described postintervention aortic WSS in patients with aortic valve and/or aorta disease. One such study compared AVR with either a stented or a stentless bioprosthesis, a mechanical valve, or autograft, against healthy controls.[17] The investigators reported a significant increase in peak systolic AA WSS in patients with bioprostheses compared with autografts and controls. WSS values were higher in our study (mean value over the 4 patients with a stented bioprosthesis, 1.8 $\pm$ 0.3 Pa; in the patient with a mechanical valve, 1.4 Pa) than in that study: stented bioprothesis, 1.4 $\pm$ 0.7 Pa (n = 14); mechanical valve, ~0.8 Pa (n = 9). This finding might be because WSS was calculated in 2D planes orthogonal to the aorta whereas we used a 3D approach throughout the aortic wall, as well as the different follow-up duration after surgery (median value in our bioprosthesis group, 380 days

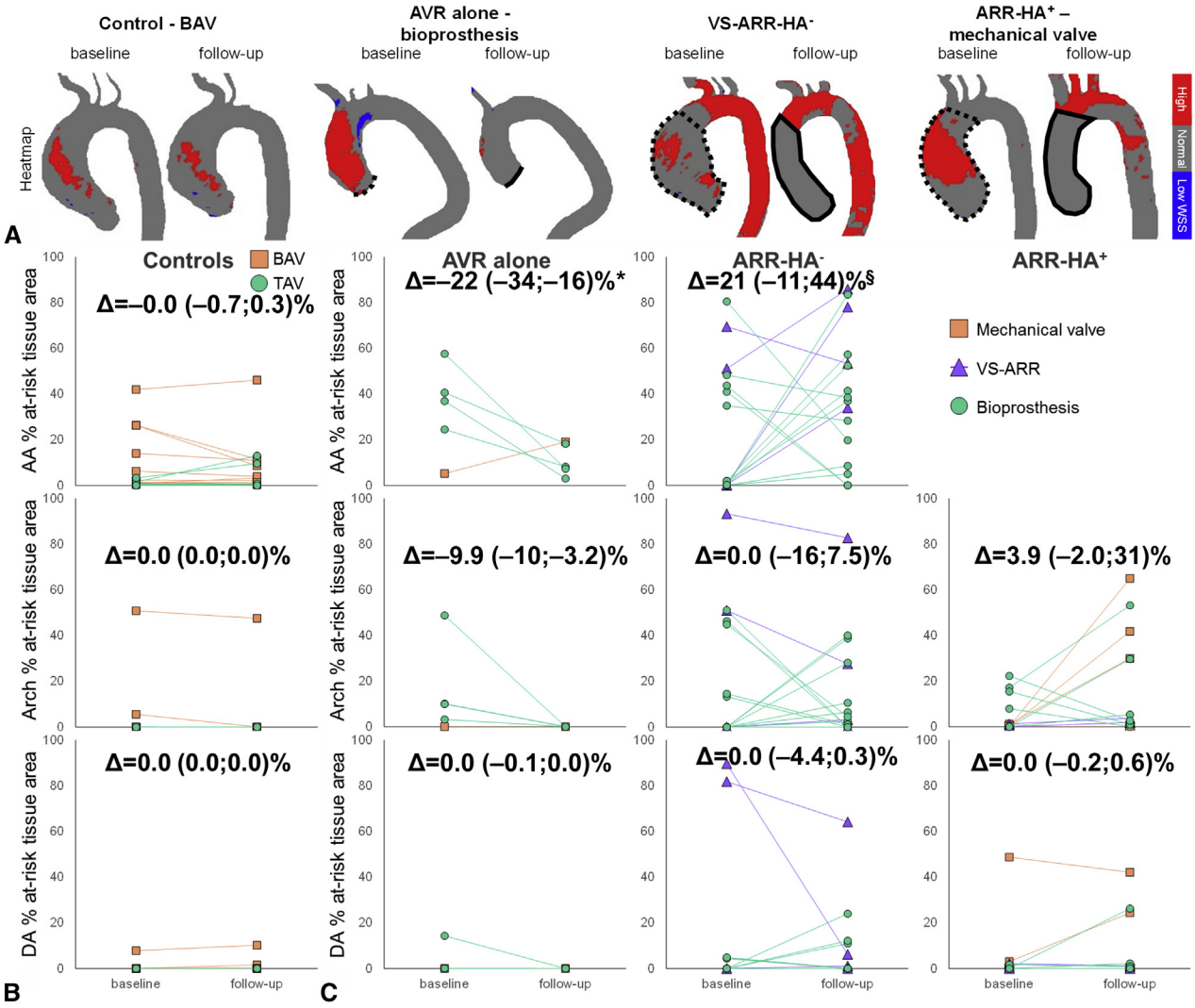

FIGURE 3. A, Baseline and follow-up aortic wall shear street (WSS) heatmap in representative control and surgery patients who underwent different intervention and aortic valve types, from left to right: bicuspid aortic valve (*BAV*) control, aortic valve replacement (*AVR*) alone with a bioprosthesis, valve-sparing aortic root replacement (*ARR*) with no hemiarch repair (*VS-ARR-HA*$^{-}$) and ARR with hemiarch repair (*ARR-HA*$^{+}$) with a mechanical valve. In surgery patient heatmaps, dotted lines indicate the area to be resected and solid lines indicate the position of the graft at baseline and follow-up, respectively. B, Evolution of percentage at-risk tissue area from baseline to follow-up in the control and (C) the surgery groups according to aortic valve type (see legends). The surgery group was further divided according to the performed intervention, from left to right: AVR alone, ARR-HA^{-}, and ARR-HA^{+}. Longitudinal changes (Δ), as defined by follow-up–baseline differences, are provided for each patient group and aortic region: ascending aorta (*AA*) (*top row*), aortic arch (*middle row*), and descending aorta (*DA*) (*bottom row*). Results were not reported in the AA for the ARR-HA^{+} group because the entire region was resected during surgery. *$P < .05$ against control group, §$P < .05$ against AVR group, with nonsignificant effects of follow-up duration. *TAV*, Tricuspid aortic valve.

[interquartile range, 321-559 days] vs 3.6 ± 2.6 years; in our mechanical valve patient, 92 days vs 7.9 ± 3.6 years). Later, the same group investigated differences in WSS after transcatheter AVR compared with conventional surgical AVR, with a stented bioprosthesis, and healthy controls.[18] The investigators found that both AVR and transcatheter AVR groups had asymmetric WSS in the mid-AA with locally increased and depressed WSS along the circumference of the aorta, whereas it was uniform around the circumference in controls. We did not look at circumferential variations of WSS in the present study, but differences after surgery should be investigated in larger patient cohorts.

Another study investigated differences in aortic WSS in patients with BAV with different leaflet fusion patterns after VS-ARR,[16] resulting in eccentric WSS patterns with higher

TABLE 3. Peak velocity in the vena contracta, as well as peak wall shear stress and percentage at-risk tissue area in the ascending aorta, aortic arch, and descending aorta at baseline and follow-up according to patient group

	No surgery (n = 20)		Surgery (n = 33)	
	Baseline	Follow-up	Baseline	Follow-up
Peak velocity (m/s), mean ± SD	1.88 ± 0.63	1.94 ± 0.64	2.95 ± 1.20*	2.50 ± 0.46*
Peak WSS (Pa), mean ± SD				
AA	1.17 ± 0.29	1.17 ± 0.34	1.50 ± 0.68	1.57 ± 0.37*
Arch	0.81 ± 0.24	0.82 ± 0.22	1.16 ± 0.40*	1.13 ± 0.35*
DA	0.79 ± 0.20	0.77 ± 0.22	0.97 ± 0.29*	0.89 ± 0.28
At-risk tissue area (%), median (interquartile range)				
AA	1.0 (0.3-4.0)	1.1 (0.1-8.8)	24 (0.2-44)	28 (8.2-52)*
Arch	0 (0-0)	0 (0-0)	1.1 (0-15)*	2.6 (0-28)*
DA	0 (0-0)	0 (0-0)	0 (0-2.1)	0 (0-2.2)

SD, Standard deviation; *WSS*, wall shear stress; *AA*, ascending aorta; *DA*, descending aorta. *$P < .05$ between surgery and no-surgery groups separately at baseline and follow-up.

WSS on the outer curvature and lower WSS on the inner curvature. Hope et al. reported aortic WSS after VS-ARR in a specific population of patients with Marfan syndrome.[15] These investigators obtained variable changes in WSS depending on the aortic region (AA or DA) and local circumferential location (anterior right wall, inner or outer curvature), between patients and healthy volunteers, as well as in a patient who developed Stanford type B dissection during follow-up, in which WSS patterns were altered.

All these studies compared postsurgical findings with either healthy volunteers or preinterventional findings obtained in different populations. To the best of our knowledge, only 2 studies reported same-patient presurgical and postsurgical WSS values. However, these studies investigated either the brachial[22] or the carotid[21] arteries, both in the setting of atherosclerosis and not aortopathy, and thus, they focused on areas of pathologically low and oscillating WSS. In addition, both of these studies used ultrasonography and a simple assumption of Poiseuille flow (based on single measurements of velocity and diameter) to calculate WSS.[21,22] Given differences in vascular territories, methodological approaches and populations between these studies and ours, it is not possible to compare besides the finding that surgery altered the expression of WSS in the vessels investigated.

This work is a first effort to report same-patient presurgical and postsurgical WSS patterns in the aorta, pooling different types of interventions (AVR and/or ARR and/or HA). We combined noninvasive 4D flow MRI data with a 3D method to compute WSS,[25] which takes full advantage of the volumetric coverage of velocities at the wall compared with approaches that are limited to 2D planes.[27] This 3D WSS method was previously shown to provide good interobserver and interscan reproducibility in healthy volunteers,[28] which was confirmed by our low interobserver variability obtained in patients including after surgery. The interobserver differences were lower compared with differences observed between before and after surgery, indicating the potential of 4D flow–derived indices to reliably detect regions with altered wall shear forces.

It was previously shown that WSS was a key hemodynamic predictor of aneurysm dilatation.[29] Until recently, aortic WSS could be assessed in vivo using only invasive techniques and was mostly estimated using computational fluid dynamics models.[29-31] However, such models are limited by their underlying idealized assumptions on blood flow, arterial geometry, and stiffness or boundary

TABLE 4. Biases (limits of agreement) for the interoperator variability of regional aortic WSS indices at baseline and follow-up in each patient group

	No surgery (n = 10)		Surgery (n = 10)	
	Baseline	Follow-up	Baseline	Follow-up
Peak WSS (Pa)				
AA	0.05 (−0.12 to 0.22)	−0.05 (−0.25 to 0.14)	0.08 (−0.21 to 0.36)	0.09 (−0.27 to 0.45)
Arch	0.01 (−0.03 to 0.04)	0.00 (−0.03 to 0.04)	0.01 (−0.07 to 0.09)	0.02 (−0.08 to 0.11)
DA	0.00 (−0.04 to 0.04)	−0.00 (−0.02 to 0.01)	−0.00 (−0.04 to 0.04)	−0.00 (−0.03 to 0.02)
At-risk tissue area (%)				
AA	0.4 (−1.1 to 1.9)	0.2 (−3.2 to 3.6)	−0.1 (−5.8 to 5.5)	−1.1 (−9.4 to 7.2)
Arch	0.8 (−4.0 to 5.6)	0.1 (−0.3 to 0.4)	0.8 (−5.4 to 7.0)	0.8 (−3.4 to 5.1)
DA	−0.0 (−0.2 to 0.2)	−0.1 (−1.2 to 1.0)	0.1 (−1.9 to 2.0)	−0.0 (−0.4 to 0.3)

WSS, Wall shear stress; *AA*, ascending aorta; *DA*, descending aorta.

conditions, which are mostly not patient specific. In addition to systolic peak WSS magnitude, we studied the extent of at-risk tissue exposed to an abnormally high WSS, as defined by the comparison with an atlas of normal WSS values. This heatmap methodology allows detection of relative changes in WSS[26] and was recently shown to correlate with resected tissue histology in patients with BAV.[19] More precisely, at-risk aortic regions of abnormally increased WSS showed significant reduction in elastin content, decreased elastin fiber thickness, and increased fragmentation, compared with regions with normal WSS in the same patient. At-risk tissue was further associated with significant changes in matrix metalloproteinase and transforming growth factor β_1 concentrations, indicating aortic wall extracellular matrix disruption. Given that the precise involvement of hemodynamics on aortopathy development is still unclear, we believe that the 4D flow MRI technique is a powerful and unique tool to investigate promising imaging biomarkers noninvasively.[7,15,17,19,24-26,32,33] The different changes observed within the patients undergoing surgery according to the intervention type suggest an opportunity to improve understanding the effects of different procedures and help surgeons decide between AVR and/or ARR with or without HA, as well as what extent of aortic area should be resected. We speculate that the increase in peak WSS and at-risk tissue area distal to the graft after root surgery is caused by the replacement of native elastic tissue by a stiff tube. Our results also suggest that resecting the aortic root versus AVR alone had more impact on WSS than further performing a hemiarch repair, in line with previous findings.[23] The decrease in WSS patterns observed after biological AVR might be caused by significantly longer follow-up in that group compared with the remaining patients undergoing ARR, as suggested by the significant effect of follow-up duration on AA peak WSS change.

The main limitation of this pilot study is the small sample size. Care must be taken regarding statistical power when dividing surgery patients according to the performed intervention or replaced aortic valve. Furthermore, surgery subgroups were heterogeneous in terms of disease, resection extent, graft size, prosthesis type, or morphology of the native aortic valve. For instance, it would be interesting to investigate if WSS pattern changes are different between patients with a native tricuspid, bicuspid, or unicuspid aortic valve after VS-ARR, especially given the potential role of hemodynamics in mediating specifically BAV aortopathy. We lack outcome data and follow-up durations were variable among patients. However, follow-up duration was significantly shorter than controls for surgery patients in whom we detected some changes in WSS patterns.

Future studies including more patients and longer follow-up at several systematic time points after surgery (1 month, 3 months, and 6 months, then yearly), as well as comparison with patient outcome, are warranted to help identify robust indices able to refine the risk of future events, such as dilatation, rupture, subsequent aortic surgery, or dissection, and to optimize the extent of aortic tissue to be resected.[23] Because our findings suggest an alteration of WSS patterns at the transition from graft to the native aorta, it might be complementary to investigate the effect of the stiff graft on downstream changes in hemodynamics.[34]

CONCLUSIONS

Our study showed the feasibility of 4D flow MRI to quantify presurgical and postsurgical aortic WSS, resulting in different responses depending on the performed intervention. Future efforts are needed to investigate the ability of our WSS indices to predict disease progression and help guide surgical resection as well as patient follow-up.

Conflict of Interest Statement

Authors have nothing to disclose with regard to commercial support.

References

1. Hiratzka LF, Bakris GL, Beckman JA, Bersin RM, Carr VF, Casey DE Jr, et al. 2010 ACCF/AHA/AATS/ACR/ASA/SCA/SCAI/SIR/STS/SVM Guidelines for the diagnosis and management of patients with thoracic aortic disease. A Report of the American College of Cardiology Foundation/American Heart Association Task Force on Practice Guidelines, American Association for Thoracic Surgery, American College of Radiology, American Stroke Association, Society of Cardiovascular Anesthesiologists, Society for Cardiovascular Angiography and Interventions, Society of Interventional Radiology, Society of Thoracic Surgeons,and Society for Vascular Medicine. *J Am Coll Cardiol*. 2010;55:e27-129.
2. Della Corte A, Body SC, Booher AM, Schaefers HJ, Milewski RK, Michelena HI, et al. Surgical treatment of BAV disease: knowledge gaps and research perspectives. *J Thorac Cardiovasc Surg*. 2014;147:1749-57. 1757.e1.
3. Melina G, De Robertis F, Gaer JA, Amrani M, Khaghani A, Yacoub MH. Mid-term pattern of survival, hemodynamic performance and rate of complications after medtronic freestyle versus homograft full aortic root replacement: results from a prospective randomized trial. *J Heart Valve Dis*. 2004;13:972-5; discussion 975-6.
4. Fairbairn TA, Steadman CD, Mather AN, Motwani M, Blackman DJ, Plein S, et al. Assessment of valve haemodynamics, reverse ventricular remodelling and myocardial fibrosis following transcatheter aortic valve implantation compared to surgical aortic valve replacement: a cardiovascular magnetic resonance study. *Heart*. 2013;99:1185-91.
5. Amat-Santos IJ, Dahou A, Webb J, Dvir D, Dumesnil JG, Allende R, et al. Comparison of hemodynamic performance of the balloon-expandable SAPIEN 3 versus SAPIEN XT transcatheter valve. *Am J Cardiol*. 2014;114:1075-82.
6. Sharma V, Deo SV, Altarabsheh SE, Cho YH, Erwin PJ, Park SJ. Comparison of the early haemodynamics of stented pericardial and porcine aortic valves. *Eur J Cardiothorac Surg*. 2015;47:4-10.
7. Keller EJ, Malaisrie SC, Kruse J, McCarthy PM, Carr JC, Markl M, et al. Reduction of aberrant aortic haemodynamics following aortic root replacement with a mechanical valved conduit. *Interact Cardiovasc Thorac Surg*. 2016;23:416-23.
8. Oechtering TH, Hons CF, Sieren M, Hunold P, Hennemuth A, Huellebrand M, et al. Time-resolved 3-dimensional magnetic resonance phase contrast imaging (4D Flow MRI) analysis of hemodynamics in valve-sparing aortic root repair with an anatomically shaped sinus prosthesis. *J Thorac Cardiovasc Surg*. 2016;152:418-27.e1.
9. Botnar R, Nagel E, Scheidegger MB, Pedersen EM, Hess O, Boesiger P. Assessment of prosthetic aortic valve performance by magnetic resonance velocity imaging. *MAGMA*. 2000;10:18-26.
10. Watanabe Y, Chevalier B, Hayashida K, Leong T, Bouvier E, Arai T, et al. Comparison of multislice computed tomography findings between bicuspid and

tricuspid aortic valves before and after transcatheter aortic valve implantation. *Catheter Cardiovasc Interv*. 2015;86:323-30.
11. Salaun E, Jacquier A, Theron A, Giorgi R, Lambert M, Jaussaud N, et al. Value of CMR in quantification of paravalvular aortic regurgitation after TAVI. *Eur Heart J Cardiovasc Imaging*. 2016;17:41-50.
12. Torii R, El-Hamamsy I, Donya M, Babu-Narayan SV, Ibrahim M, Kilner PJ, et al. Integrated morphologic and functional assessment of the aortic root after different tissue valve root replacement procedures. *J Thorac Cardiovasc Surg*. 2012;143:1422-8.
13. Kidher E, Cheng Z, Jarral OA, O'Regan DP, Xu XY, Athanasiou T. In-vivo assessment of the morphology and hemodynamic functions of the BioValsalva composite valve-conduit graft using cardiac magnetic resonance imaging and computational modelling technology. *J Cardiothorac Surg*. 2014;9:193.
14. Tanweer O, Wilson TA, Metaxa E, Riina HA, Meng H. A comparative review of the hemodynamics and pathogenesis of cerebral and abdominal aortic aneurysms: lessons to learn from each other. *J Cerebrovasc Endovasc Neurosurg*. 2014;16:335-49.
15. Hope TA, Kvitting JP, Hope MD, Miller DC, Markl M, Herfkens RJ. Evaluation of Marfan patients status post valve-sparing aortic root replacement with 4D flow. *Magn Reson Imaging*. 2013;31:1479-84.
16. Stephens EH, Hope TA, Kari FA, Kvitting JP, Liang DH, Herfkens RJ, et al. Greater asymmetric wall shear stress in Sievers' type 1/LR compared with 0/LAT BAVs after valve-sparing aortic root replacement. *J Thorac Cardiovasc Surg*. 2015;150:59-68.
17. von Knobelsdorff-Brenkenhoff F, Trauzeddel RF, Barker AJ, Gruettner H, Markl M, Schulz-Menger J. Blood flow characteristics in the ascending aorta after aortic valve replacement–a pilot study using 4D-flow MRI. *Int J Cardiol*. 2014;170:426-33.
18. Trauzeddel RF, Lobe U, Barker AJ, Gelsinger C, Butter C, Markl M, et al. Blood flow characteristics in the ascending aorta after TAVI compared to surgical aortic valve replacement. *Int J Cardiovasc Imaging*. 2016;32:461-7.
19. Guzzardi DG, Barker AJ, van Ooij P, Malaisrie SC, Puthumana JJ, Belke DD, et al. Valve-related hemodynamics mediate human bicuspid aortopathy: insights from wall shear stress mapping. *J Am Coll Cardiol*. 2015;66:892-900.
20. Crouch G, Bennetts J, Sinhal A, Tully PJ, Leong DP, Bradbrook C, et al. Early effects of transcatheter aortic valve implantation and aortic valve replacement on myocardial function and aortic valve hemodynamics: insights from cardiovascular magnetic resonance imaging. *J Thorac Cardiovasc Surg*. 2015;149:462-70.
21. Irace C, Gnasso A, Cirillo F, Leonardo G, Ciamei M, Crivaro A, et al. Arterial remodeling of the common carotid artery after aortic valve replacement in patients with aortic stenosis. *Stroke*. 2002;33:2446-50.
22. Horn P, Stern D, Veulemans V, Heiss C, Zeus T, Merx MW, et al. Improved endothelial function and decreased levels of endothelium-derived microparticles after transcatheter aortic valve implantation. *EuroIntervention*. 2015;10:1456-63.
23. Malaisrie SC, Duncan BF, Mehta CK, Badiwala MV, Rinewalt D, Kruse J, et al. The addition of hemiarch replacement to aortic root surgery does not affect safety. *J Thorac Cardiovasc Surg*. 2015;150:118-24.e2.
24. Rose MJ, Jarvis K, Chowdhary V, Barker AJ, Allen BD, Robinson JD, et al. Efficient method for volumetric assessment of peak blood flow velocity using 4D flow MRI. *J Magn Reson Imaging*. 2016;44:1673-82.
25. Potters WV, van Ooij P, Marquering H, vanBavel E, Nederveen AJ. Volumetric arterial wall shear stress calculation based on cine phase contrast MRI. *J Magn Reson Imaging*. 2015;41:505-16.
26. van Ooij P, Potters WV, Nederveen AJ, Allen BD, Collins J, Carr J, et al. A methodology to detect abnormal relative wall shear stress on the full surface of the thoracic aorta using four-dimensional flow MRI. *Magn Reson Med*. 2015;73:1216-27.
27. Stalder AF, Russe MF, Frydrychowicz A, Bock J, Hennig J, Markl M. Quantitative 2D and 3D phase contrast MRI: optimized analysis of blood flow and vessel wall parameters. *Magn Reson Med*. 2008;60:1218-31.
28. van Ooij P, Powell AL, Potters WV, Carr JC, Markl M, Barker AJ. Reproducibility and interobserver variability of systolic blood flow velocity and 3D wall shear stress derived from 4D flow MRI in the healthy aorta. *J Magn Reson Imaging*. 2016;43:236-48.
29. Pasta S, Rinaudo A, Luca A, Pilato M, Scardulla C, Gleason TG, et al. Difference in hemodynamic and wall stress of ascending thoracic aortic aneurysms with bicuspid and tricuspid aortic valve. *J Biomech*. 2013;46:1729-38.
30. Arzani A, Suh GY, Dalman RL, Shadden SC. A longitudinal comparison of hemodynamics and intraluminal thrombus deposition in abdominal aortic aneurysms. *Am J Physiol Heart Circ Physiol*. 2014;307:H1786-95.
31. Lei M, Archie JP, Kleinstreuer C. Computational design of a bypass graft that minimizes wall shear stress gradients in the region of the distal anastomosis. *J Vasc Surg*. 1997;25:637-46.
32. Bogren HG, Buonocore MH, Follette DM. Four-dimensional aortic blood flow patterns in thoracic aortic grafts. *J Cardiovasc Magn Reson*. 2000;2:201-8.
33. Kvitting JP, Ebbers T, Wigstrom L, Engvall J, Olin CL, Bolger AF. Flow patterns in the aortic root and the aorta studied with time-resolved, 3-dimensional, phase-contrast magnetic resonance imaging: implications for aortic valve-sparing surgery. *J Thorac Cardiovasc Surg*. 2004;127:1602-7.
34. Aquaro GD, Briatico Vangosa A, Toia P, Barison A, Ait-Ali L, Midiri M, et al. Aortic elasticity indices by magnetic resonance predict progression of ascending aorta dilation. *Eur Radiol*. 2017;27:1395-403.

Key Words: wall shear stress, aortic valve replacement, aortic root replacement, hemiarch repair, perioperative, 4D flow MRI

APPENDIX E1

Magnetic Resonance Imaging Acquisitions

Magnetic resonance imaging (MRI) examinations were conducted on MAGNETOM 1.5T Aera or Avanto (n = 94) and 3T Skyra (n = 12) scanners (Siemens Medical Systems, Erlangen, Germany), after injection of a gadolinium-based contrast agent (0.03 mol/kg Ablavar [Lantheus Medical Imaging, N. Billerica, Mass]; or 0.1-0.2 mmol/kg Gadavist or Magnevist [Bayer, Leverkusen, Germany]; or 0.1-0.2 mmol/kg Multihance [Bracco Diagnostics Inc, Township, NJ]).

Prospectively electrocardiogram (ECG)–gated 4D flow MRI (three-dimensional time-resolved phase-contrast magnetic resonance imaging with three-directional velocity encoding) data were acquired in a sagittal volume encompassing the thoracic aorta. Respiration gating was achieved by means of a 16-mm acceptance window size navigator placed on the lung-liver interface. Parallel imaging (GRAPPA) along the phase encoding direction (y) was used with a reduction factor R = 2 (24 reference lines) to accelerate the acquisition. Other sequence parameters were as follows: repetition time, 4.8 ± 0.1 ms; echo time, 2.4 ± 0.1 ms; flip angle, 15°; acquisition matrix, 160×80-100; isotropic pixel in-plane spacing, 2.18 ± 0.13 mm [range, 2.125-2.6875 mm]; slice thickness, 2.88 ± 0.32 mm [range, 2.4-3.8 mm]; 2 k-space segments per cardiac time frame; temporal resolution, 38.3 ± 0.65 ms [range, 36.8-40 ms]; number of slices, 23-36; receiver bandwidth, 445-460 Hz/pixel; encoding sensitivity Venc, 150-300 cm/s depending on the presence and severity of aortic valve stenosis.

Assessment of Left Ventricle and Aortic Valve Function as Well as Aortic Dimensions

Left ventricle (LV) end-systolic and end-diastolic volumes were measured with conventional contouring of ECG-gated cine balanced steady-state free precession (bSSFP) short-axis images covering the LV and including the papillary muscles and chamber trabecula using QMass v7.2 (Medis, Leiden, The Netherlands), to calculate stroke volume and ejection fraction.

Aortic valve morphology and function were determined using cine bSSFP and two-dimensional phase-contrast images obtained at the level of the aortic valve. Bicuspid aortic valve morphology was classified according to Sievers classification.[E1] Aortic valve stenosis and regurgitation severity was classified as none, trace, mild, moderate, or severe according to published guidelines.[E2]

Aortic diameter measurements were obtained from contrast-enhanced magnetic resonance angiography images at the sinuses of Valsalva (SOV) and midascending aorta (mid-AA) using the open-source, free DICOM (Digital Imaging and Communications in Medicine) medical image viewer Horos (2015, http://www.horosproject.org/; based On OsiriX). SOV diameter was the maximal value among the 3 sinus-to-sinus measurements, including the external walls. Mid-AA diameter was the maximal value over 2 orthogonal measurements in a reformatted plane orthonormal to the aorta, including the external walls.[E3]

4D Flow MRI Data Analysis

For each baseline and follow-up 4D flow data set, preprocessing was first applied using a previously described MATLAB program (The Mathworks, Natick, Mass),[E4] including eddy current correction, background noise suppression, and velocity aliasing unwrapping. A 3D angiogram (phase-contrast magnetic resonance angiography) was computed by multiplying absolute velocity by magnitude images and averaging over all cardiac phases,[E4] to segment the aortic volume (Mimics, Materialize, Leuven, Belgium) and subsequently mask the flow velocities (Figure 1, *A*).

E-References

E1. Sievers HH, Schmidtke C. A classification system for the BAV from 304 surgical specimens. *J Thorac Cardiovasc Surg*. 2007;133:1226-33.

E2. Erbel R, Aboyans V, Boileau C, Bossone E, Bartolomeo RD, Eggebrecht H, et al. 2014 ESC Guidelines on the diagnosis and treatment of aortic diseases: Document covering acute and chronic aortic diseases of the thoracic and abdominal aorta of the adult. The Task Force for the Diagnosis and Treatment of Aortic Diseases of the European Society of Cardiology (ESC). *Eur Heart J*. 2014;35:2873-926.

E3. Trinh B, Dubin I, Rahman O, Ferreira Botelho MP, Naro N, Carr JC, et al. Aortic volumetry at contrast-enhanced magnetic resonance angiography: feasibility as a sensitive method for monitoring BAV aortopathy. *Invest Radiol*. 2017;52:216-22.

E4. Schnell S, Entezari P, Mahadewia RJ, Malaisrie SC, McCarthy PM, Collins JD, et al. Improved semiautomated 4D flow MRI analysis in the aorta in patients with congenital aortic valve anomalies versus tricuspid aortic valves. *J Comput Assist Tomogr*. 2016;40:102-8.

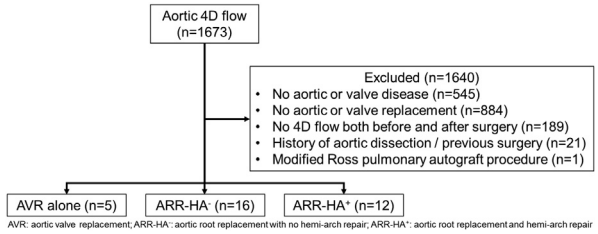

FIGURE E1. Consort flow diagram for retrospective cohort identification from an institutional database of aortic 4D flow MRI examinations.